

## **Mechanical Design and Analysis of an Electron Beam Scraper/Spoiler at the Advanced Photon Source**

**Jie Liu, Leonard Morrison, Geoff Waldschmidt, Jeffrey Dooling**

Advanced Photon Source, Argonne National Laboratory

9700 S. Cass Avenue, Argonne, IL 60439, USA

jliu@aps.anl.gov; morrison@aps.anl.gov;

Waldschm@aps.anl.gov; dooling@aps.anl.gov

**Abstract** - In the past, two versions of an electron beam scraper were installed at the S37 straight section of the Advanced Photon Source (APS) storage ring. Both experienced beam induced damage during operations (Dooling, 2013). Studies had shown that the mechanical design and scraper material selection were responsible for the failures. Analyses revealed that Titanium alloy and aluminum alloy may be the two best options for the beam interaction material (Dooling, 2014). A new scraper/spoiler has been designed as a platform to test these two materials, as well as incorporating optimizations to reduce the impedance and Radio Frequency (rf) energy deposition from the beam. In this paper, the mechanical design of the scraper/spoiler and the analysis of the heat load due to beam interaction, rf heating, and synchrotron radiation is presented. Finite element thermal analyses are also presented and discussed.

**Keywords:** electron beam scraper, electron beam spoiler, finite element analysis, thermal analysis, mechanical design

### **1. Introduction**

The horizontal scraper installed at sector 37 straight section of the Advanced Photon Source (APS) storage ring at Argonne National Laboratory (ANL) was proposed to protect the downstream insertion devices from Touschek-scattered and dumped beam (Borland, 2004). It was installed and tested as a beam spoiler/beam dump and to intercept electron beam halo and transient beam loss during injection (Dooling, 2011). It also served as a diagnostic to probe the edges of the beam and measure the physical aperture when stored beam was lost (Dooling, 2013). Two versions of scrapers were installed and tested and both experienced beam-induced damage during operation (Dooling, 2013 and Xiao, 2013). The temperature of the vacuum chamber rose rapidly and caused a vacuum leak at the upstream and downstream flanges. After being removed from the storage ring, it was also observed that the absorption material of the scraper was seriously damaged due to high temperature increases from beam dumps. Simulations indicated that tungsten and copper were not suitable options as absorbing material. Instead, aluminum (Al) or titanium (Ti) alloy are the two best options (Dooling, 2014). Meanwhile, a new concept for a spoiler-absorber design had been proposed and analyzed (Borland, 2012). Based on these studies, a modified scraper/spoiler has been designed to test the new concept and materials. In the new design, the scraper is functioning as a spoiler rather than a beam dump since the deposited energy in the absorbing material due to beam interaction was significantly less than the total stored energy in the beam. This new design also reduced the impedance and rf energy deposition which had previously caused excessively high temperature in the vacuum chamber.

## 2. Mechanical design of the scraper/spoiler

Based on physics requirements, the scraper blade is a rectangular block of overall length 160 mm with two 20 mm by 20 mm chamfers at both ends in the beam direction as shown in figure 1(d). The height is 39.91 mm and is constrained by the beam chamber dimension. A critical gap of  $0.9 \pm 0.1$  mm must be maintained on all sides, between the scraper blade and the aperture in the vacuum chamber to reduce the effects of electromagnetic fields that can become trapped. The blade is designed to allow for the evaluation of the different plates. A 5 mm thick plate made of either Ti alloy or Al alloy will be tested in each case. The scraper/spoiler consists of three main components: the vacuum chamber, the blade subassembly, and the drive system, as shown in Fig. 1.

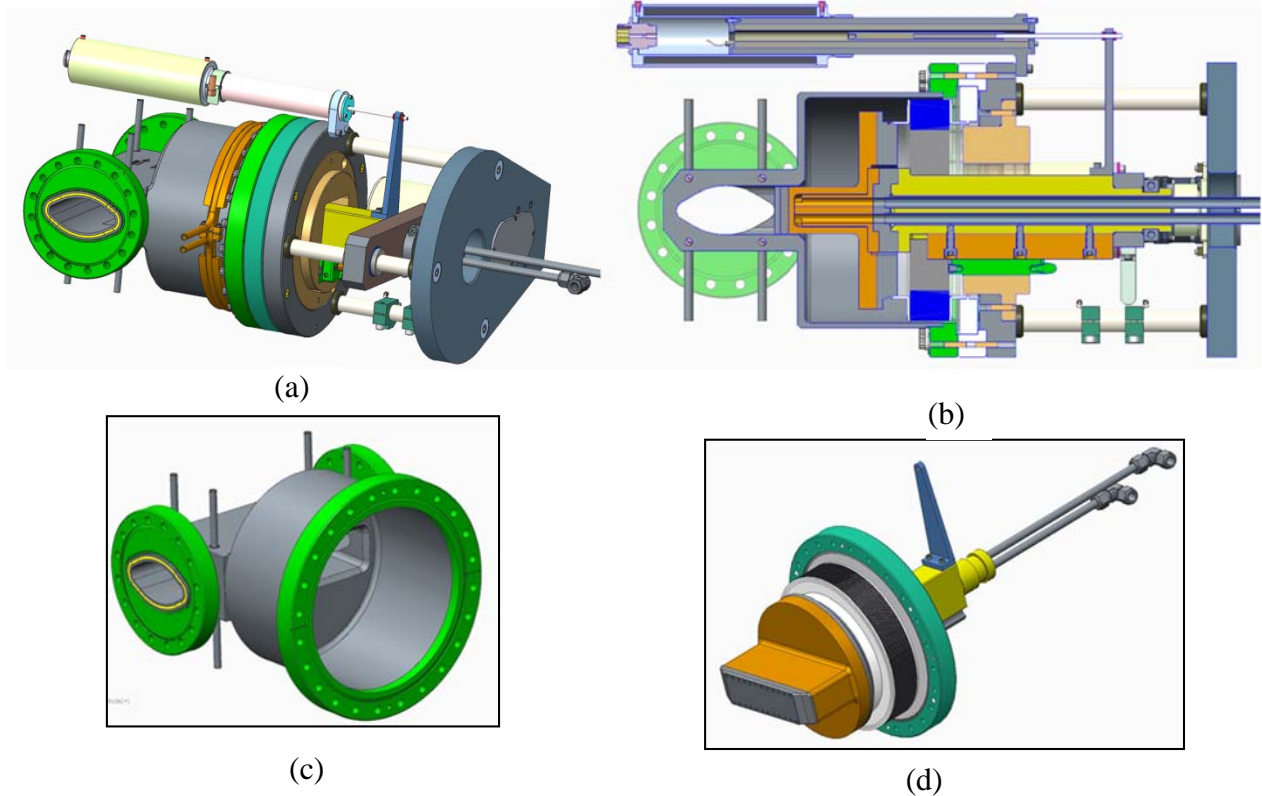


Fig. 1 Mechanical design and components of the scraper/spoiler: (a) Full scraper assembly with vacuum chamber, blade subassembly and vacuum chamber, (b) Cross-sectional view of full scraper assembly, (c) Vacuum chamber, and (d) Scraper blade subassembly with bellows and cooling lines.

The vacuum chamber houses the scraper blade, supports the drive system, and provides a mounting interface with the upstream and downstream chambers. To ensure that the intercepting face of the blade is parallel with the beam trajectory, the beam chamber and the scraper housing are machined with high precision. Four cooling channels will be machined along the electron beam chamber.

The blade subassembly includes the interchangeable scraper/spoiler insert, scraper blade with cooling system, and a rail for the precision guideway. The scraper/spoiler insert will be bolted onto the body of the blade with twenty-four M2 screws. A layer of high conductive silver film may be added to the interface to improve the thermal conductance. Once testing of the scraper is completed, the insert will be integrated into the blade body. To ensure the critical gap between the vacuum chamber and the blade, the blade assembly is mounted onto a high precision guideway and rail system for translation in and out of

the beam. The blade is a brazed assembly of OFE copper sandwiched between Ti alloy on the beam side to interface with inserts and 304SS on the opposite end to interface with stainless bellow. A cooling system is designed into the blade assembly.

### 3. Finite Element Thermal Analyses

Besides geometrical and material requirements, there are also restrictions on the temperature rise of the scraper/spoiler. The vacuum chamber body and cylindrical flange temperature cannot exceed 100 °C and the temperature of the insert cannot exceed its melting point. There are three sources of heat load for the scraper: (1) energy deposition due to the electron beam absorption by the insert; (2) RF induced heat load due to the impedance, and (3) synchrotron radiation from the upstream bending magnet. The final temperature rise is the result of the collective heating due to these three heat sources.

#### 3. 1. Electron Beam deposition

Initial electron loss distributions are generated by the accelerator tracking code, ELEGANT (Borland, 2000). The output from ELEGANT is then used by the particle-matter interaction program MARS (Mokhov, 1995). A beam dump results in the total loss of storage ring charge in a relatively short period of time. In the present case, 368 nC of 7 GeV electrons are distributed equally among 24 bunches. The electrons circulate in the 1104-m circumference storage ring vacuum chamber making one revolution or turn every 3.68 μs. In the most severe case, the store is lost in as little as 3 turns (11 μs). At 100 mA, the total stored charge is 2578 J. Other fill patterns are used in the SR; however, the 24-bunch pattern has been shown to cause the most damage to the scraper. The total energy deposited on the insert for 100mA beam current was calculated to be 49 J for aluminum and 141 J for titanium due to the different radiation lengths and densities of the alloys. A comparison of these quantities is presented in Table 1.

Table 1. Comparison of Al6063T6 and Ti6Al4V

Material	Radiation length, $X_0$ (g/cm <sup>2</sup> )	Density, $\rho$ (g/cm <sup>3</sup> )	Length, $t=X_0/\rho$ (cm)
Al6063T6	24.3	2.7	8.99
Ti6Al4V	16.8	4.43	3.79

Simulating the effect of a beam dump, energy deposition values in the insert are recorded using 50μm transverse voxel sizes (Dooling, 2014). The insert contained 25 voxels in the longitudinal direction (parallel to the beam) with voxel length of 5mm. For the thermal simulations, this transverse particle distribution was converted into volumetric heat generation and applied to each voxel. The maximum temperature rise due to electron beam energy deposition was found to be approximately 1051 °C for Ti6Al4V and 468 °C for Al6063T6. The melting point of Ti6Al4V and Al6063T6 are about 1650°C and 600 °C, respectively. As a consequence, the temperature rise by other sources cannot exceed 300 °C and 100°C for Ti alloy and Al alloy, respectively. MARS employs a temperature-dependent specific heat based on the amount of energy deposited in a given voxel to determine the temperature rise. Specific heat can vary appreciably from room-temperature values. Maximum longitudinal temperature excursion profiles for both aluminum and titanium alloys are compared for constant (diamond) and temperature-dependent specific heat (square). In both cases the temperature-dependent results yield lower peak values. The total energy deposited in each longitudinal segment is also shown in Fig. 2. The results from ANSYS agree with that from MARS very well, as shown in Fig 3(a).

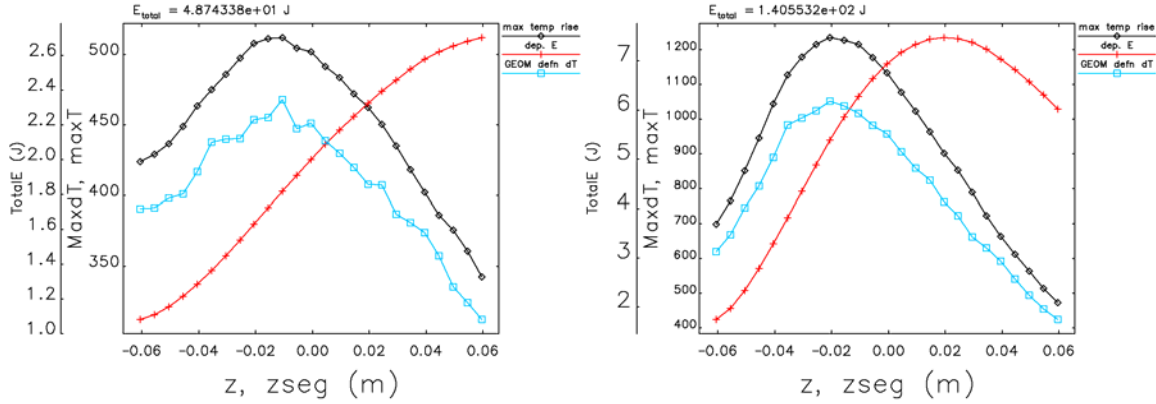


Fig. 2 Peak insert temperature excursion and energy deposition profiles in: (a) Al alloy, and (b) Ti alloy

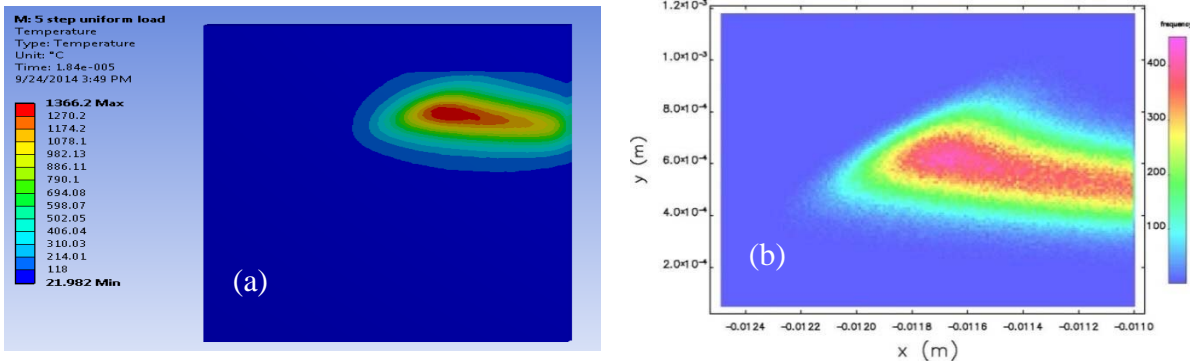


Fig. 3(a) shows the temperature rise and distribution at the peak cross-section caused by particle absorption in the Ti6Al4V insert. Fig. 3(b) shows the corresponding particle density contour from MARS simulations.

These results imply that the scraper would not be able to withstand 150 mA of beam current because the melting point would be exceeded at 150 mA. However, the maximum temperature occurs about 0.8 mm below the surface. The surface temperature would not reach melting point. Transient analysis shows that the maximum temperature would drop about 600 °C in less than 10 ms. More simulations and tests need be done to study how this is going to affect the allowable maximum beam current.

### 3. 2. RF heat load and induced temperature rise

Electron bunches circulate the APS storage ring at a rate of 270 kHz and interact with the scraper assembly to an extent that is dependent upon the perturbation introduced by the scraper. This new design has been mechanically and electrically optimized to reduce this interaction by tailoring the shape of the scraper blade, minimizing the clearance between the scraper and vacuum chamber, and eliminating any significant resonant effect.

A broadband time-domain simulation with a 10 mm bunch length is shown in Fig. 4(a) where the scraper blade was fully extended. The strongest resonances are visible at frequencies below 4.5 GHz which is the TM11 mode cutoff frequency of the vacuum chamber. The power lost by a 150 mA beam was also calculated using frequency-domain modal analysis and is summarized in Fig. 4(b). The total power lost by the beam was estimated as 250 W where 140 W was distributed as a traveling wave and the remaining 110 W was trapped within the scraper assembly. Due to the relatively low conductivity of

stainless steel, the quality factor of the generated rf modes was low to prevent any resonant effect between consecutive bunches in the bunch train.

The total power loading of 250W was used as a conservative estimate for the thermal analysis of the scraper where all beam-generated rf power was assumed to be trapped within the scraper. Cooling channels were located along the length of the vacuum chamber, inside the scraper blade assembly, and circumferentially on the external cylindrical housing of the scraper to keep the maximum temperature excursion of 100<sup>o</sup>C at all vacuum flanges. The distribution of rf losses on the surfaces of the scraper from each mode was summed and used as the spatially distributed loading for the thermal simulations. Fig. 5 shows the results of the thermal analysis for the inner and outer components of the scraper where the nominal water temperature was set to 25.6<sup>o</sup>C. The overall temperature is shown to remain well below 100<sup>o</sup>C throughout the volume. The temperature rise of the titanium insert was less than 20<sup>o</sup>C.

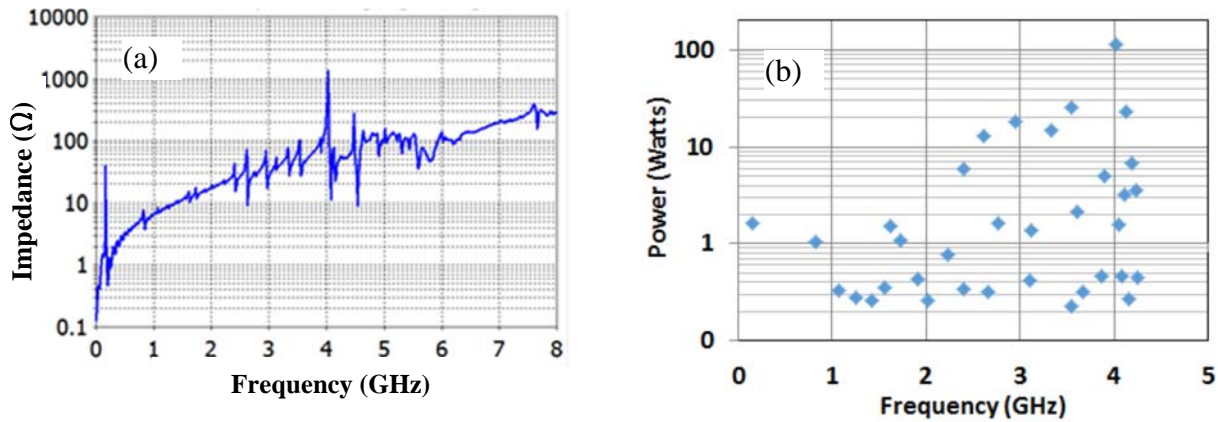


Figure 4: Beam interaction with scraper assembly: (a) Impedance of the scraper based on a time-domain analysis of the wakefield with a 10mm bunch length and (b) Power loss distribution at significant rf modes due to a 150 mA beam.

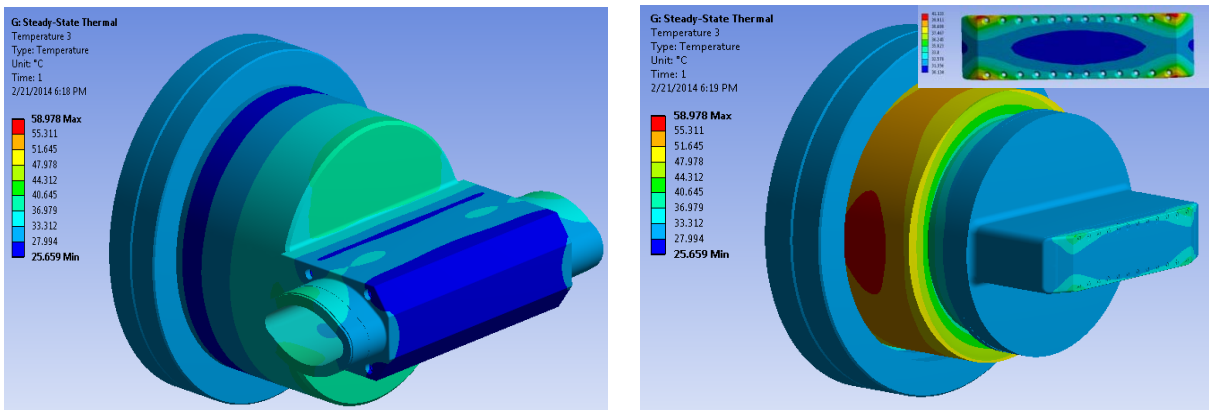


Figure 5: Thermal distribution along scraper assembly due to rf interaction with the beam: (a) Outer assembly and (b) Inner assembly with inset of titanium insert.

### 3. 3. Synchrotron radiation heat load and temperature rise

The heat load from synchrotron radiation in the worst mis-steering case is 20.3W at 150mA beam current. Fig. 6 shows the temperature rise due to synchrotron radiation on the scraper body. The

occurrence of temperature rise is mostly on the chamfer surface and would not add significantly to the maximum temperature of the scraper body.

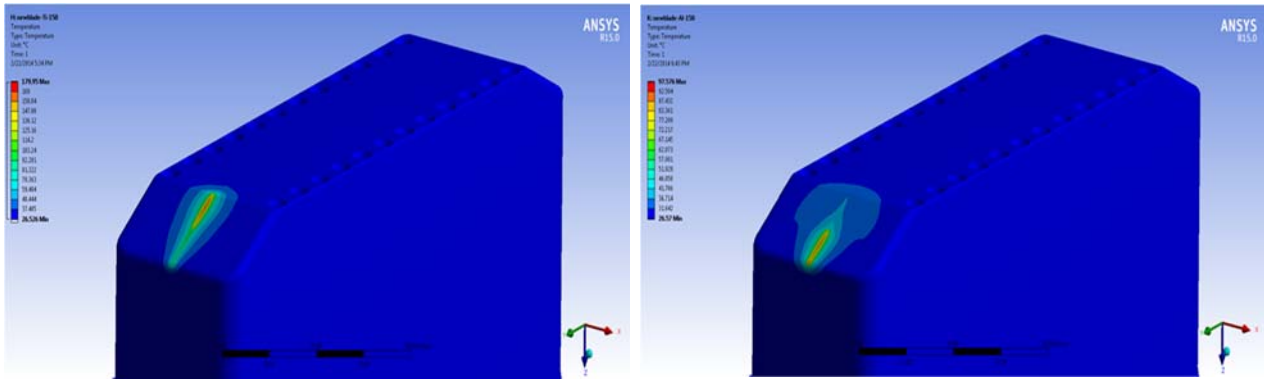


Fig. 6 temperature rise of the scraper blade due to synchrotron radiation

#### 4. Summary

The mechanical design of a modified scraper/spoiler is presented in this paper. The design comprises three components: the vacuum chamber, the scraper/spoiler blade, and the drive system. Intensive simulation works was done to ensure adequate cooling was added to ensure proper functioning of the scraper/spoiler. The analyses results were presented and discussed. Results have shown that the design will meet the design requirements for 100 mA of beam current. However, more work needs be done to prove that it can be applied for 150 mA of beam current.

#### Acknowledgements

Work supported by the U.S. Department of Energy, Office of Science, under contract number DEAC02-06CH11357.

#### References

- A. Xiao (2013), Sector 37 Scraper commissioning and test plan, APS technical notes, AOP-TN-2013-031
- J.C. Dooling (2013), Energy deposition in the sector 37 scraper of the advanced photon source storage ring, Proceedings of PAC2013, Pasadena, CA, USA, 1361-1363
- J. C. Dooling (2014), Material considerations for the sector 37 scraper, APS technical notes, AOP-TN-2014-016
- M. Borland (2004), Simulation of scattering from scrapers in the APS, APS technical notes, OAG-TN-2004-061
- M. Borland (2000), LS-287, Advanced Photon Source
- N.V. Mokhov (1995), "The Mars Code System User's Guide", Fermilab-FN-628; N.V.
- S.I. Striganov (2007), "MARS15 Overview", Fermilab-Conf-07/008-AD; in Proc. of Hadronic Shower Simulation Workshop, Fermilab, September 2006, AIP Conf. Proc. 896, pp. 50-60; <http://www-ap.fnl.gov/MARS/>